

# Andreev-Lifshitz conjecture revisited for a few electrons on a square lattice I

Georgios Katomeris, Franck Selva and Jean-Louis Pichard

CEA/DSM, Service de Physique de l'État Condensé, Centre d'Études de Saclay, 91191, Gif sur Yvette cedex, France

the date of receipt and acceptance should be inserted later

**Abstract.** A quantum theory of defects in solids has led Andreev and Lifshitz to conjecture the existence of a vacancy-solid phase taking place at zero temperature between the Fermi liquid and the Wigner solid. In this and a succeeding paper, we re-visit this issue using  $N$  spinless fermions interacting via a  $U/r$  Coulomb repulsion on a two dimensional  $L \times L$  square lattice with periodic boundary conditions and nearest neighbor hopping  $t$ . This paper is restricted to the magic number  $N = 4$  for which a square Wigner molecule is formed when  $U$  increases and to the size  $L = 6$  suitable for exact numerical diagonalizations. When the Coulomb energy to kinetic energy ratio  $r_s = UL/(2t\sqrt{\pi N})$  reaches a value  $r_s^F \approx 10$ , there is a level crossing between ground states of different momenta. Above  $r_s^F$ , the mesoscopic crystallization proceeds through an intermediate regime ( $r_s^F < r_s < r_s^W \approx 28$ ) where unpaired fermions with a reduced Fermi energy co-exist with a strongly paired, nearly solid assembly. We suggest that this is the mesoscopic trace of the vacancy-solid phase proposed by Andreev and Lifshitz. When a random substrate is included, the level crossing at  $r_s^F$  is avoided and gives rise to a lower threshold  $r_s^F(W) < r_s^F$  where two usual approximations break down: the Wigner surmise for the distribution of the first energy excitation and the Hartree-Fock approximation for the ground state.

**PACS.** 71 27 Strongly correlated electron systems – 73.21.L Quantum dots: electron states – 67 80 Quantum crystals

## 1 Introduction

A basic question in quantum many body theory is to know how one goes from independent particle motion towards collective motion when one decreases the density  $n_s$  of a system of charged particles repelling each other via a  $U/r$  Coulomb repulsion. As introduced long ago by Wigner, the factor  $r_s$ , defined as the radius  $r$  of the volume enclosing a single particle in units of the Bohr radius  $a_B$ , governs this crossover. Quantum mechanical effects are important when  $r_s$  is small, and become more and more negligible when  $r_s$  becomes large. Since  $r_s \propto 1/\sqrt{n_s}$  in two dimensions, the quantum limit of a Fermi liquid is obtained at large densities  $n_s$ . In the dilute limit, the quantum effects disappear and the charges crystallize, forming a Wigner solid of minimum electrostatic energy. A calculation of the electrostatic energy of different crystalline arrays shows that the hexagonal array minimizes the energy in the  $2d$  continuum. However, in a square lattice model with periodic boundary conditions (BCs), the symmetry of the Wigner solid is restricted and the formation of a square crystalline array is favored.

Before studying this quantum-classical crossover in a mesoscopic lattice model, let us mention that it is usually assumed [1,2] that a single liquid-solid transition takes place at  $r_s \approx 37$  in the continuous  $2d$  thermodynamic

limit. For instance, this single transition was obtained by fixed node quantum Monte Carlo calculations [1,3], allowing to study a few hundreds of electrons and to vary their number for estimating the finite size effects. The fixed node approximation is made to avoid the negative weights that would be generated otherwise by antisymmetric states, and gives an upper bound to the exact ground state energy. Two nodal structures have been considered, given by two Slater-Jastrow wave functions adapted to describe the weak coupling Fermi liquid (nodal structure of a Slater determinant of plane waves) and the strong coupling Wigner solid (nodal structure of a Slater determinant of localized site orbitals). The existence of a single transition separating the Fermi liquid from the Wigner solid is therefore a consequence of the assumed nodal structures, and not the result of a calculation. When the spin degrees of freedom are included, the existence of an intermediate polarized liquid phase separating the unpolarized liquid and the Wigner solid is still debated [4].

### 1.1 2d metal and related issues

The motivation to re-visit nowadays charge crystallization in  $2d$  Coulomb systems is fourfold. Firstly, it becomes possible to create  $2d$  gases of charges in high quality field effect devices and to decrease by a gate the carrier density  $n_s$ .

for obtaining a large factor  $r_s$ . Doped semi-conductors [5] (Si-Mosfet, Ga-As heterostructures, Si-Ge quantum wells) or undoped organic crystals [6] can be now used to study how one goes in two dimensions from a Fermi liquid towards a Wigner crystal. Secondly, the direct observation of the Wigner crystal being difficult, one can nevertheless measure the conductance of the dilute  $2d$  electron gas at different densities as a function of the temperature, of the bias voltage, of a parallel magnetic field, etc. Remarkably, those transport measurements, first done [5] by Kravchenko et al in high quality Si-MOSFETs, show the existence of an unexpected metal-insulator transition (MIT) when the gate voltage varies and the dilute limit is reached. A similar MIT was later observed [5] using Ga-As heterostructures, Si-Ge quantum wells and undoped organic crystals. This observation of a low temperature metallic behavior for typically  $3 \dots 6 < r_s < 9 \dots 30$  (the largest ratios characterizing the cleaner samples) raises the question of a possible intermediate phase, which should be neither a Fermi glass of localized particles (Anderson insulator), nor a correlated Wigner solid (pinned insulating crystal). Thirdly, the formation of a mesoscopic Wigner molecule can be also nowadays studied using a quantum dot[7] with a few electrons or a few ions [8] trapped by electric and magnetic fields. Increasing the size of the trap yields [9] a crossover from independent-particle towards collective motion. Lastly, an unexplained intermediate regime was numerically observed [10,11,12] in studying the persistent currents carried by the ground state and the low energy excitations of mesoscopic disordered clusters. Both experiments and numerics give unexplained low energy behaviors for similar intermediate values of the ratio  $r_s$ .

## 1.2 Vacancy-solid phase

In this study, we consider fully polarized electrons and ignore possible magnetic transitions. For avoiding uncontrolled assumptions, we consider a system which is small enough to allow exact numerical diagonalization, but where the lattice effects and the finite size corrections are important. Those two effects have been studied in details in Ref. [13] for two electron square lattices. Our main goal is to characterize as precisely as possible the ground state for intermediate ratios  $r_s$ , in order to see if a small lattice model does not exhibit the mesoscopic signature of an intermediate phase separating the solid from the liquid, where the solid and the fluid would coexist. Such a vacancy-solid phase was indeed suggested [14] by Andreev and Lifshitz if the zero point motions of certain defects become sufficient to form waves propagating inside the solid. Castaing and Nozières have later considered [15] such a possibility for spin polarized  $\text{He}^3$ . The statistics of the defects depend on their nature. For simple vacancies in the crystal, their statistics is given by the statistics of the particles out of which the solid is made. If the defects are bosons, they may form a condensate, giving rise to a superfluid coexisting with the solid. This supersolid phase is discussed in certain bosonic models [16]. If the defects

are fermions, they may form a Fermi liquid [17] coexisting with the solid, such that the system is neither a solid, nor a liquid. Two kinds of motion are possible in it; one possesses the properties of motion in an elastic solid, the second possesses the properties of motion in a liquid.

If one considers the quantum melting of the solid from the dilute limit (large  $r_s$ ), the nature of the relevant defects is not an easy question. One can imagine a particle being put into an interstitial site of the Wigner lattice, creating a vacancy-interstitial pair at a certain electrostatic cost  $\delta U$ . A model assuming such defects has been recently proposed [18] for describing addition spectra in quantum dots. Classically, this vacancy-interstitial pair remains localized. But quantum tunneling may lead to delocalization of the defects and to the appearance of a band of defects of finite width  $B_d$  which increases when  $r_s$  decreases. When  $B_d$  exceeds  $\delta U$ , one can imagine two possibilities: either the total quantum melting [3] of the Wigner crystal (simple solid-liquid transition), or a partial melting leading to the persistence of a floppy crystal with delocalized defects. If a delocalized defect appears in the quantum crystal, the crystal remains perfectly periodic, but the number of crystal lattice sites becomes smaller to the total number of particles.

If one considers charge crystallization from the other limit, where the density  $n_s$  is large (small  $r_s$ ), one can argue that the interaction will create correlated pairs of particles near the Fermi surface, but will not reorganize the one particle states well below the Fermi surface. Such a possibility has been proposed by Bouchaud et al [19] for liquid  $\text{He}^3$ . Moreover, they have developed a variational approach, based on a fixed number of fermions BCS wave function, having a different nodal structure than the Jastrow-Slater nodal structures considered in Ref. [1]. In this picture, the system is thought as made of unpaired fermions with a *reduced* Fermi energy, co-existing with a strongly paired, nearly solid assembly. Furthermore, it was stressed that the inhomogeneous vacancy solid - first introduced by Andreev and Lifshitz - would be a good candidate to describe this new phase. To the concept of a crystal with a reduced number of crystal lattice sites, as discussed by Andreev and Lifshitz from the solid limit, corresponds the concept of unpaired fermions with a reduced Fermi energy, as discussed by Bouchaud et al from the liquid limit.

Since it was observed in Ref. [11] that the low energy levels do not obey Wigner-Dyson statistics for disordered clusters at intermediate ratios  $r_s$ , the existence of low energy collective excitations in the clean limit can be suspected. For this reason, we have studied the same clusters as in Refs. [10,11] without random substrate and we have observed at intermediate  $r_s$  a floppy correlated solid coexisting with a liquid of unpaired particles. This conclusion is supported by a study of the projection of the ground state (GS) onto a combination of Slater determinants (SDs) built out from plane waves and from site orbitals. The plane wave SDs are given by the low energy levels of same total momentum  $\mathbf{K}$  as the intermediate GS, and correspond to unpaired fermions with a

reduced Fermi energy. The site SDs describe the Wigner solid molecule and its small fluctuations. Since the GS is given by the combination of unpaired fermions and of a floppy Wigner molecule for  $r_s^F \approx 9.3 < r_s < r_s^W \approx 28$  in the studied system, we suggest that this is the mesoscopic trace of the macroscopic state discussed in Refs. [14] and [19]. The study of the GS response to various perturbations (Aharonov-Bohm flux, pinning well) and of the distributions of the different inter-particle spacings allows us to give a few remarkable properties of the intermediate regime. Eventually, we consider the effect of disorder and give further evidence of the existence of a first threshold  $r_s^F(W)$  where correlation effects occur: (i) the breakdown of the Hartree-Fock approximation for the ground state and (ii) the breakdown of Wigner-Dyson level repulsion for the first excitation.

## 2 Lattice model

We consider fully polarized electrons (i.e. spinless fermions), having symmetric spin wave functions and antisymmetric orbital wave functions, free to move in an  $L \times L$  lattice with periodic BCs, and interacting via a  $U/\mathbf{r}$  Coulomb repulsion. The Hamiltonian reads

$$H = -t \sum_{\langle \mathbf{i}, \mathbf{j} \rangle} c_{\mathbf{i}}^\dagger c_{\mathbf{j}} + \sum_{\mathbf{i}} v_{\mathbf{i}} n_{\mathbf{i}} + \frac{U}{2} \sum_{\mathbf{i} \neq \mathbf{j}} \frac{n_{\mathbf{i}} n_{\mathbf{j}}}{|\mathbf{r}_{\mathbf{i}\mathbf{j}}|} \quad (1)$$

where  $\mathbf{i}, \mathbf{j}$  label the lattice sites,  $\langle \mathbf{i}, \mathbf{j} \rangle$  means  $\mathbf{i}$  nearest neighbor to  $\mathbf{j}$ ,  $c_{\mathbf{i}}^\dagger, c_{\mathbf{i}}$  are the creation, annihilation operators of a spinless fermion at the site  $\mathbf{i}$ ;  $n_{\mathbf{i}} = c_{\mathbf{i}}^\dagger c_{\mathbf{i}}$  is the occupation number at the site labeled by the vector  $\mathbf{i} = (i_x, i_y)$ . The vector  $\mathbf{r}_{\mathbf{i}\mathbf{j}}$  is defined as the shortest vector going from the site  $\mathbf{i}$  to the site  $\mathbf{j}$  in a square lattice with periodic BCs ( $r_x$  and  $r_y \leq L/2$ ).  $t = \hbar^2/(2ma^2)$  is the hopping term,  $a$  the lattice spacing,  $v_{\mathbf{i}}$  the site potentials which are randomly distributed in the interval  $[-W/2, W/2]$  and  $U = e^2/(\epsilon a)$  the Coulomb interaction between two fermions separated by  $a$  in a medium of dielectric constant  $\epsilon$ .

This work is restricted to a detailed study of the case  $N = 4$  and  $L = 6$ , corresponding to a filling factor  $\nu = N/L^2 = 1/9$ .  $N = 4$  is a ‘magic’ number for which at large values of  $U$ , the  $3 \times 3$  square Wigner molecule is commensurate with the imposed  $6 \times 6$  square lattice. The  $r_s$  factor, defined in the continuum as

$$r_s = \frac{1}{\sqrt{\pi n_s a_B}} \quad (2)$$

for a carrier density  $n_s$  and a Bohr radius  $a_B = \hbar^2 \epsilon / (me^2)$ , becomes in a lattice model

$$r_s = \frac{U}{2t\sqrt{\pi\nu}} \quad (3)$$

since  $\hbar^2/(2ma^2) \rightarrow t$ ,  $e^2/(\epsilon a) \rightarrow U$ . and  $n_s = \nu/a^2$ .

A  $L \times L$  continuous  $2d$  torus having infinitely more degrees of freedom than a mere  $6 \times 6$  lattice, one cannot compare the obtained lattice behaviors to those obtained assuming a continuous space, as in Ref. [1], without further investigations. Nevertheless, appropriately defined observables should only depend on the value of the dimensionless ratio  $r_s$ , up to certain finite size corrections. This has been checked [13] for two particle square lattices when the fluctuation  $\Delta r$  of the distance  $r$  between the two particles is larger than the lattice spacing  $a$ . Calculating  $\Delta r$  in powers of  $t/U$ , one finds [13] that a correlated lattice regime takes place when  $r_s$  exceeds a threshold value  $r_s^* \approx 100$  when  $N = 2$  and  $L = 6$ . Below  $r_s^*$ ,  $r_s \propto UL/t$  is the relevant scaling variable, up to certain finite size corrections of order  $1/L^2$ . Above  $r_s^*$ , one has a lattice regime where  $r_s$  is not a relevant scaling variable. Assuming that the threshold value  $r_s^*$  does not vary very much when one goes from  $N = 2$  to  $N = 4$ , one can expect to have a four particle Wigner molecule free of important lattice effects as far as  $r_s < r_s^* \approx 100$  when  $L = 6$ .

## 3 The non disordered lattice

When there is no disorder ( $W = 0$ ),  $\mathbf{k} = (k_x, k_y)$  being the one particle momentum, it is more convenient to write  $H$  using the Fourier transforms of the creation and annihilation operators. One has the relations

$$c_{\mathbf{j}} = \frac{1}{L} \sum_{\mathbf{k}} d_{\mathbf{k}} e^{i\mathbf{k}\cdot\mathbf{j}}, \quad (4)$$

and

$$d_{\mathbf{k}} = \frac{1}{L} \sum_{\mathbf{j}} c_{\mathbf{j}} e^{-i\mathbf{k}\cdot\mathbf{j}}. \quad (5)$$

which yield

$$H = \sum_{\mathbf{k}} d_{\mathbf{k}}^\dagger d_{\mathbf{k}} \varepsilon(\mathbf{k}) + \sum_{\mathbf{q}, \mathbf{k}_1, \mathbf{k}_2} V(\mathbf{q}) d_{\mathbf{k}_2 + \mathbf{q}}^\dagger d_{\mathbf{k}_1 - \mathbf{q}}^\dagger d_{\mathbf{k}_1} d_{\mathbf{k}_2} \quad (6)$$

where

$$\varepsilon(\mathbf{k}) = -2t (\cos k_x + \cos k_y) \quad (7)$$

and

$$V(\mathbf{q}) = \frac{U}{2L^2} \sum_{\mathbf{j} \neq 0} \frac{e^{i\mathbf{q}\cdot\mathbf{j}}}{|\mathbf{r}_{\mathbf{j}0}|} \quad (8)$$

In the eigenbasis of the non interacting system (eigenvectors  $d_{\mathbf{k}_1}^\dagger d_{\mathbf{k}_2}^\dagger d_{\mathbf{k}_3}^\dagger d_{\mathbf{k}_4}^\dagger |0\rangle$ ,  $|0\rangle$  being the vacuum state), the Hamiltonian matrix is block diagonal, each block being characterized by the same conserved total momentum  $\mathbf{K} = \sum_{i=1}^4 \mathbf{k}_i$ . Only the non interacting states having in common two  $\mathbf{k}$ s out of four can be coupled by the interaction inside a  $\mathbf{K}$  sub-block. Therefore, each  $\mathbf{K}$  sub-block is a sparse matrix which can be exactly diagonalized using the Lanczos algorithm.

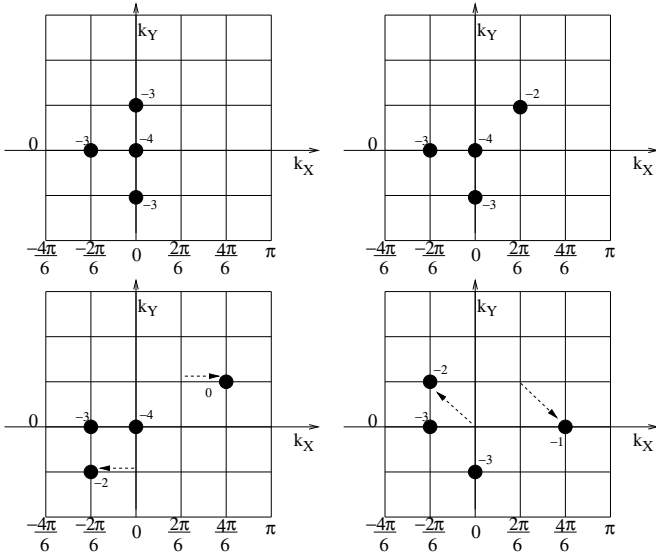


**Fig. 1.** Low kinetic energy plane wave SDs in momentum space of coordinates  $(k_x, k_y)$ : 1 GS  $|K_0(\beta)\rangle$  with  $\mathbf{K} \neq 0$  (upper left), together with 3 plane wave SDs of  $\mathbf{K} = 0$  and of low energies: one of the 4  $|K_1(\beta)\rangle$  of energy  $-12t$  (upper right), and two of the 16  $|K_4(\gamma)\rangle$  of energy  $-9t$  (lower right and left) directly coupled by the two body interaction to the  $|K_1(\beta)\rangle$  shown in the upper right figure. A circle means that the state  $(k_x, k_y)$  is occupied, its energy being indicated in units of  $t$ .

### 3.1 The free Fermi limit

When  $U = 0$ , the states are then  $N_H$  plane wave SDs  $d_{\mathbf{k}_1}^\dagger d_{\mathbf{k}_2}^\dagger d_{\mathbf{k}_3}^\dagger d_{\mathbf{k}_4}^\dagger |0\rangle$ .  $N_H = M!/(N!(M-N)!) = 58905$  for  $M = L^2 = 36$  and  $N = 4$ . The low energy levels without interaction are by increasing energies:

- 4 GSSs  $|K_0(\beta)\rangle$  of energy  $E_0(U=0) = -13t$  and of momenta  $\mathbf{K}_0 \neq 0$ .
- 25 first excitations of energy  $E_1(U=0) = -12t$ ,
- 64 second excitations of energy  $E_2(U=0) = -11t$  and of momenta  $\mathbf{K}_2 \neq 0$ .
- 180 third excitations of energy  $E_3(U=0) = -10t$  and of momenta  $\mathbf{K}_3 \neq 0$ .
- 384 fourth excitations of energy  $E_4(U=0) = -9t$ .

If one considers the low energy states of total momentum  $\mathbf{K} = 0$ , some of them being shown in Fig. 1, one finds by increasing energy:

- 4 SDs  $|K_1(\beta)\rangle$  ( $\beta = 1, \dots, 4$ ) of energy  $-12t$ , corresponding to a particle at an energy  $-4t$  with  $\mathbf{k}_1 = (0,0)$ , two particles at an energy  $-3t$  and a fourth particle of energy  $-2t$ ; plus a single SD  $|K_1(0)\rangle$  with 4 particles of energy  $-3t$ .
- 16 SDs  $|K_4(\gamma)\rangle$  ( $\gamma = 1, \dots, 18$ ) of energy  $-9t$  given by 8 SDs where the particles have energies  $-4t, -3t, -2t, 0t$  respectively and by 8 other SDs where the particles have energies  $-3t, -3t, -2t, -t$  respectively. Note that the  $|K_4(\gamma)\rangle$  are directly coupled to the  $|K_1(\beta)\rangle$  by the pairwise interaction.

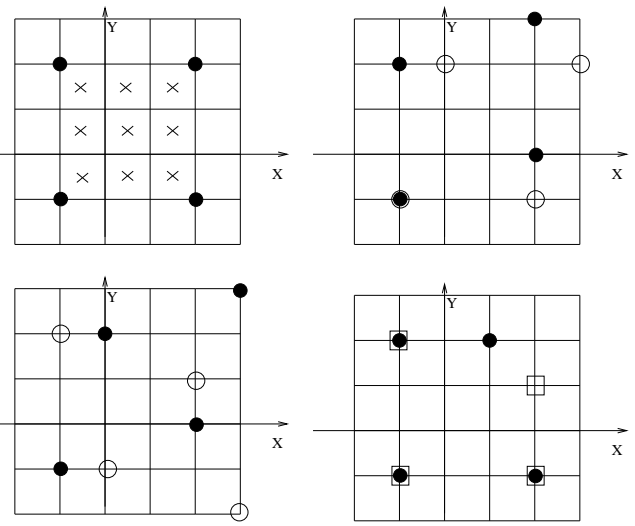


**Fig. 2.** Low Coulomb energy site SDs in real space of coordinates  $(x, y)$ : one  $|S\rangle$  with its 9 possible centers of mass (upper left), two  $|P_2\rangle$  (upper right), two  $|P_3\rangle$  (lower left) and two  $|DS\rangle$  (lower right), which give by successive translations one  $|S(\mathbf{K}=0)\rangle$ , two  $|P_2(\mathbf{K}=0, J)\rangle$ , two  $|P_3(\mathbf{K}=0, J)\rangle$  and two out of four  $|DS(\mathbf{K}=0, J)\rangle$  respectively. The two others  $|DS(\mathbf{K}=0, J)\rangle$  are obtained by successive translations of the square deformed at the opposite corner.

### 3.2 The correlated lattice limit

When  $t = 0$ , the translational invariance is broken and the states are  $N_H$  Slater determinants  $c_i^\dagger c_j^\dagger c_k^\dagger c_l^\dagger |0\rangle$  built out from the site orbitals. The configurations  $ijkl$  correspond to the  $N_H$  different patterns characterizing 4 different sites of the  $L \times L$  square lattice. The configurations of low electrostatic energy are respectively:

- 9 square configurations  $|S\rangle$  of side  $b = 3$  and of energy  $E_0(t=0) \approx 1.80U$ ,
- 36 parallelograms  $|P_1\rangle$  of sides  $(3, \sqrt{10})$  and of energy  $\approx 1.85U$ ,
- 36 other parallelograms  $|P_2\rangle$  of sides  $(\sqrt{10}, \sqrt{10})$  and of energy  $\approx 1.97U$ ,
- 144 deformed squares  $|DS\rangle$  obtained by moving a single site of a square  $|S\rangle$  by one lattice spacing and of energy  $\approx 2U$ .

Some of those low energy site SDs are shown in Fig. 2. When an infinitesimal hopping term  $t$  is included, one must delocalize the site SDs in order to restore translational invariance and to have eigenstates of given quantized total momenta  $\mathbf{K}$ . For instance, the 9 squares  $|S\rangle$  give 9 eigenstates of momentum  $\mathbf{K}$

$$|S(\mathbf{K})\rangle = \frac{1}{L^2} \sum_{j_x, j_y=1}^L \exp i(\mathbf{K} \cdot \mathbf{j}) T_j |S\rangle \quad (9)$$

where

$$T_j |S\rangle = c_{(j_x, j_y)}^\dagger c_{(j_x, j_y+3)}^\dagger c_{(j_x+3, j_y)}^\dagger c_{(j_x+3, j_y+3)}^\dagger |0\rangle. \quad (10)$$

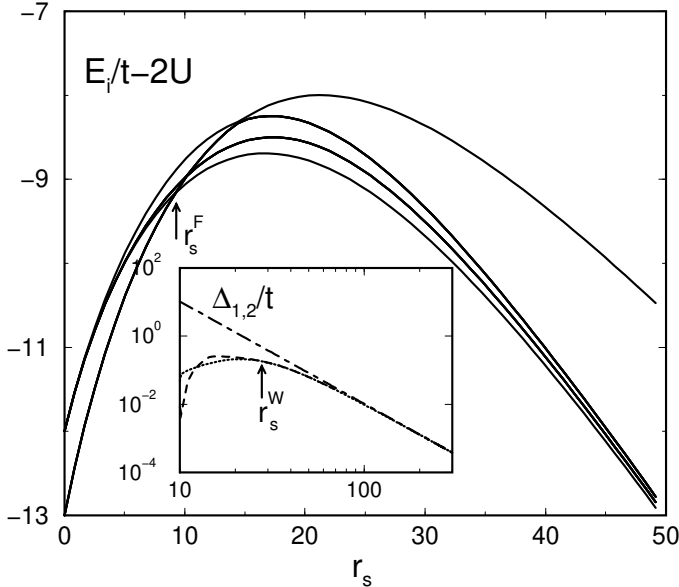


**Fig. 3.** As a function of  $r_s$ , low energy part of the spectrum exhibiting a level crossing at  $r_s^F$ . Inset: two first level spacings  $\Delta_1/t$  (dashed) and  $\Delta_2/t$  (dotted) and the perturbative result  $3Dr_s^{-3}$  (dot-dashed).

The possible momenta for the  $|S(\mathbf{K})\rangle$  are given by  $(K_x, K_y) = 2\pi(p_x, p_y)/(L/2)$ .

If we consider the low energy states of total momentum  $\mathbf{K} = 0$  when  $r_s \rightarrow \infty$ , one finds by increasing energy the following delocalized site SDs:

- 1 delocalized square  $|S(\mathbf{K} = 0)\rangle$ ,
- 2 delocalized parallelograms  $|P_1(\mathbf{K} = 0, J)\rangle$  ( $J = 1, 2$ ) obtained from the 36  $|P_1\rangle$ ,
- 2 delocalized parallelograms  $|P_2(\mathbf{K} = 0, J)\rangle$  ( $J = 1, 2$ ) obtained from the 36  $|P_2\rangle$ ,
- 4 delocalized deformed squares  $|DS(\mathbf{K} = 0, J)\rangle$  obtained from the 144  $|DS\rangle$ .

### 3.3 Level crossing at $r_s^F$ and charge crystallization at $r_s^W$

The low energy part of the spectrum is shown in Fig. 1 as a function of  $r_s$ . If we follow the 4 GSs of energy  $-13t$  at  $r_s = 0$  ( $\mathbf{K}_0 \neq 0$ ), one can see a first level crossing at  $r_s^F \approx 10$  with a non degenerate level ( $\mathbf{K}_0 = 0$ ) which becomes the GS above  $r_s^F$ , followed by two other crossings with two other sets of 4 levels with  $\mathbf{K}_I \neq 0$ . When  $r_s$  is large, 9 levels coming from  $E_1(r_s = 0)$  have a smaller energy than the 4 levels coming from  $E_0(r_s = 0)$ . Since the degeneracies are (9, 36, 36) when  $t = 0$ , these 9 states give the 9 square molecules  $|S\rangle$  when  $r_s \rightarrow \infty$ . The degeneracies ordered by increasing energy become (1, 4, 4, 4) instead of (4, 25, 64) for  $r_s = 0$ .

To describe large  $r_s$ , one can use degenerate perturbation theory and study how the degeneracy of the 9  $|S\rangle$  is removed by terms  $\propto t/U \propto r_s^{-1}$ . The centers of mass  $\mathbf{R}$  of the 9  $|S\rangle$  are located on the periodic  $3 \times 3$  square

lattice sketched in Fig. 2. For large  $r_s$ , one has a single rigid molecule free to move on this restricted lattice, with a hopping term  $T \propto tr_s^{-3}$  and a quantized momentum  $\mathbf{K} = 2\pi/(L/2)(p_x, p_y)$ . Taking into account also the corrections to the diagonal matrix elements, one obtains for the 9 first energies  $E_0(\mathbf{K})$  in the limit  $r_s \rightarrow \infty$

$$\frac{E_0(\mathbf{K})}{t} = E_D - 2\frac{T}{t}(\cos K_x(I) + \cos K_y(I)). \quad (11)$$

$E_D = Ar_s + B/r_s + C/r_s^3$  and  $T/t = D/r_s^3$  ( $A \approx 2.13$ ,  $B \approx -70.81$ ,  $C \approx -18763$  and  $D \approx 3464$ ).  $E_D$  comes from the small vibrations of the rigid molecule while  $8T$  is the band width of its zero point fluctuations. The degeneracies are 1, 4, 4 respectively.

Four observations can be drawn from this  $t/U$  expansion.

- The ground state must exhibit a level crossing since the total momentum  $\mathbf{K} = 0$  when  $r_s \rightarrow \infty$  (lowest quantized kinetic energy for the center of mass of a rigid square molecule) while  $\mathbf{K} \neq 0$  when  $r_s \rightarrow 0$  (incomplete filling of the Fermi shell  $-3t$ ). Is this GS level crossing a general feature? As explained in Ref. [20]  $\mathbf{K} \neq 0$  at large  $r_s$  for  $N = 3$  and  $L = 6$ , and there is no GS level crossing while there is one if  $N = 3$  and  $L = 8$ . When the spins are included, the GS level crossing disappears for  $N = 4$  and  $L = 6$ .  $\mathbf{K} = 0$  at large  $r_s$  for any  $L \times L$  square lattice with a filling factor  $\nu = 1/9$ . For  $L = N = 9$ , the Fermi shell  $-2t$  is totally filled,  $\mathbf{K} = 0$  at  $r_s = 0$  and momentum conservation does not yield a GS level crossing, in contrast to the case  $L = 12$  and  $N = 16$  where the Fermi shell is incompletely filled. As we see, the existence of a GS level crossing depends on  $L$  and  $N$  and may not have a particular significance. In this work, we have studied the true GS, taking the subspaces of  $\mathbf{K} \neq 0$  below  $r_s^F$ , the subspace of  $\mathbf{K} = 0$  above  $r_s^F$ . One could have preferred to study the GS inside the subspace of  $\mathbf{K} = 0$  for all the values of  $r_s$ , to find that the onset of correlation effects which we observe at  $r_s^F$  as we will see later should occur at a possibly smaller threshold in the  $\mathbf{K} = 0$  subspace.
- In the inset of Fig. 3, one can see that the  $t/U$  expansion gives an accurate description of the 9 first energies above a relatively large value  $r_s \approx 100$ . As explained in Ref. [13], this  $t/U$  expansion is characteristic of a correlated lattice regime where the fluctuations of the charges around the equilibrium Wigner lattice sites are strongly restricted by the imposed lattice. This lattice expansion has to be distinguished from the large  $r_s$  expansion of a continuous model, where the oscillatory motion of the electrons around the Wigner crystal equilibrium positions gives [21] for the GS energy an expansion in powers of  $1/\sqrt{r_s}$ .
- Though the  $t/U$  lattice expansion ceases to be accurate below  $r_s \approx 100$ , the 9 low energy states begin to have the structure of the spectrum of a single massive particle in a  $3 \times 3$  lattice (two equal energy spacings  $\Delta_1 = \Delta_2$  characterizing the 3 first sets of states with degeneracies 1, 4, 4 respectively) at a lower value

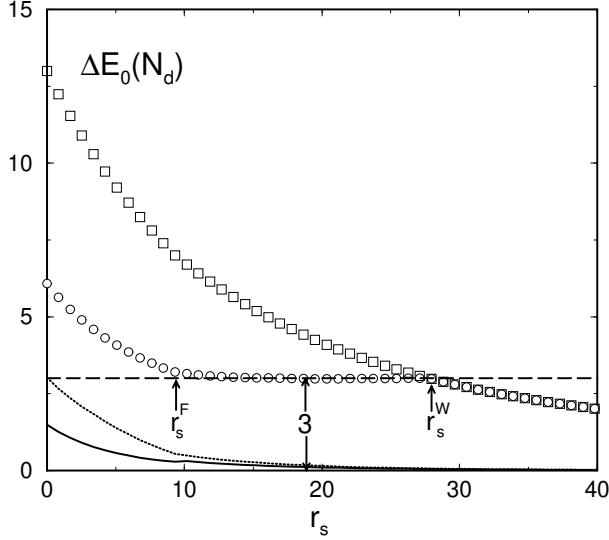


**Fig. 4.** Errors  $\Delta E_0(N_d) = (E_0(N_d) - E_0)/t$  as a function of  $r_s$ :  $d = 1$  (thick line),  $d = \sqrt{2}$  (dotted line),  $d = 2$  ( $\circ$ ),  $d = \sqrt{5}$  ( $\square$ )).

$r_s^W \approx 28$ . This structure means that the system remains essentially a rigid square molecule with its 9 quantized modes for the motion of the center of mass down to  $r_s^W$ . To create a defect in this square molecule costs a high energy available in the 10<sup>th</sup> excitation only. This is why we identify  $r_s^W$  as the threshold value for the mesoscopic crystallization, above a first threshold  $r_s^F$  and below a higher threshold  $r_s \approx 100$  where the lattice  $t/U$  expansion becomes valid.

#### 3.4 Truncated site basis

The  $N_H$  site SDs  $c_i^\dagger c_j^\dagger c_k^\dagger c_l^\dagger |0\rangle$  correspond to the  $N_H$  different patterns characterizing 4 different sites  $ijkl$  of the  $L \times L$  square lattice. If we order those configurations by the smallest distance  $d$  between two sites,  $N_d$  denoting the number of configurations with inter-site spacings larger than  $d$ , one has  $N_1 = 27225$ ,  $N_{\sqrt{2}} = 9837$ ,  $N_2 = 2709$ ,  $N_{\sqrt{5}} = 81$  configurations having a smallest inter-site spacing  $> d$ , out of  $N_H = 58905$  configurations. The two thresholds  $r_s^F$  and  $r_s^W$  can be also detected if one calculates the GS energy  $E_0(N_d)$  of the truncated Hamiltonian written using the site SDs basis restricted to  $N_d$  site SDs and if we consider the error  $\Delta E_0(N_d) = (E_0(N_d) - E_0)/t$  made using this truncation for having the exact GS energy  $E_0$ . As shown in Fig. 4, the error  $\Delta E_0(N_1)$  becomes small above  $r_s^F$ , while the error  $\Delta E_0(N_{\sqrt{5}}) = E_0(t=0) - E_0$  for all values of  $r_s$ . The error  $\Delta E_0(N_2)$  has a very interesting behavior. As  $r_s$  increases,  $\Delta E_0(N_2)$  first decreases up to  $r_s \approx r_s^F$ , then exhibits a very remarkable plateau for  $r_s^F < r_s < r_s^W$ , taking a value  $\approx 3t$  independently of  $r_s$ , before decreasing as  $\Delta E_0(N_{\sqrt{5}})$  above  $r_s^W$ . This plateau suggests that the GS for intermediate  $r_s$  is composed of a floppy molecule which can be projected onto the  $N_2$  site SDs adapted to describe it, plus an unpaired fermion of

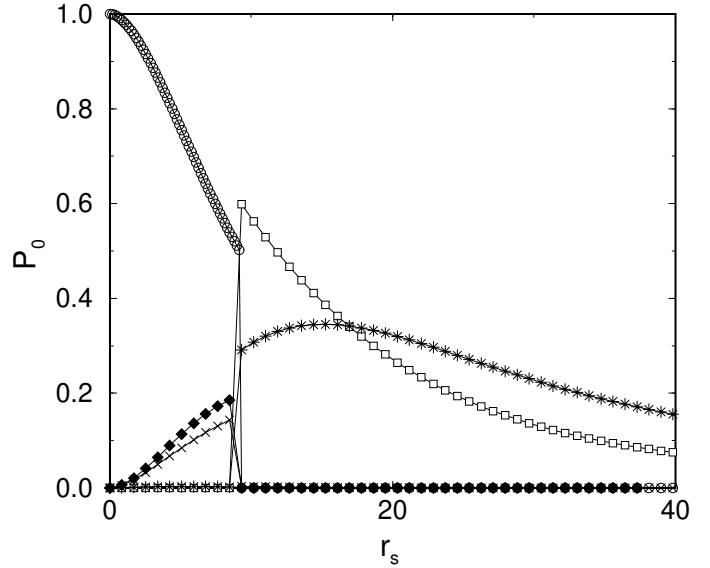


**Fig. 5.** GS Projections  $P_0^0$  ( $\circ$ ),  $P_0^1$  ( $\square$ ),  $P_0^2$  ( $\blacklozenge$ ),  $P_0^3$  ( $\times$ ) and  $P_0^4$  ( $*$ ) onto plane wave SDs of low energy when  $r_s \rightarrow 0$

kinetic energy  $\approx -3t$  which is not included in this truncated subspace since it is delocalized. Very remarkably, this energy turns out to be the energy of a particle at the Fermi surface of the non interacting system.

#### 3.5 GS projections onto plane waves

To understand further the nature of the GS between  $r_s^F$  and  $r_s^W$ , we have projected the GS wave functions  $|\Psi_0(r_s)\rangle$  over the low energy plane wave SDs appropriate to describe unpaired fermions. As shown in Fig. 5, below  $r_s^F$ , a  $\mathbf{K} \neq 0$  GS has a large projection  $P_0^0(r_s)$  over the  $U = 0$  GS of same  $\mathbf{K}$  and begins to have a smaller projection  $P_0^2(r_s)$  over the second excitations of the non interacting system of same  $\mathbf{K}$ . Above  $r_s^F$ , the non degenerate GS with  $\mathbf{K} = 0$  has of course no projection onto the plane wave SDs of  $\mathbf{K} \neq 0$ , but has a large projection

$$P_0^1(r_s) = \sum_{\beta=1}^4 |\langle \Psi_0(r_s) | K_1(\beta) \rangle|^2 \quad (12)$$

which is equally distributed over the 4 low energy states  $|K_1(\beta)\rangle$  of  $\mathbf{K} = 0$  and a non negligible projection

$$P_0^4(r_s) = \sum_{\gamma=1}^{16} |\langle \Psi_0(r_s) | K_4(\gamma) \rangle|^2 \quad (13)$$

over the 16 previously defined  $|K_4(\gamma)\rangle$  of  $\mathbf{K} = 0$  which are directly coupled by the interaction to the  $|K_1(\beta)\rangle$ .

One concludes that a significant part of the system remains an excited liquid above  $r_s^F$ , described by a large projection  $P_0 = P_0^1 + P_0^4$  over a few combinations of low energy unpaired fermions. Due to the GS level crossing, the intermediate GS has to be described from the  $\mathbf{K} = 0$

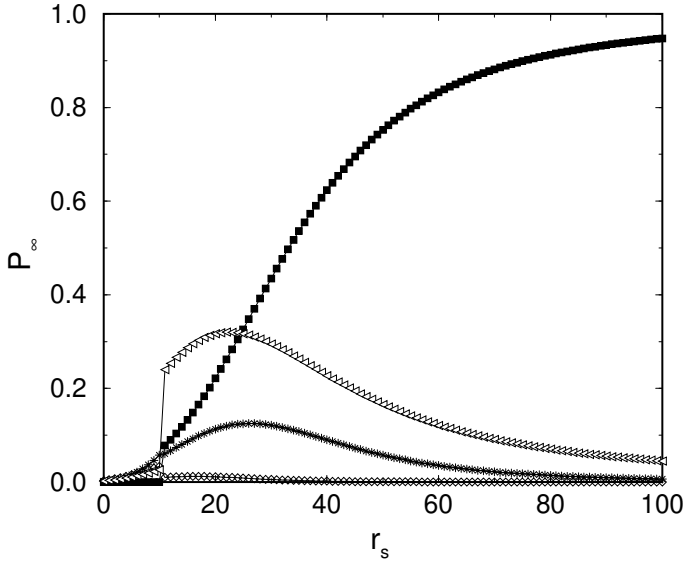


**Fig. 6.** GS projection  $P_\infty^0(r_s)$  (■),  $P_\infty^1(r_s)$  (\*),  $P_\infty^2(r_s)$  (◊) and  $P_\infty^3(r_s)$  (△) onto the first  $\mathbf{K} = 0$  delocalized site SDs of low energy when  $r_s \rightarrow \infty$ .

Fermi sea and not from the  $\mathbf{K} \neq 0$  Fermi sea. Since this projection is only partial, only a part of the system is made of unpaired fermions, in agreement with the concept proposed by Bouchaud et al of a *reduced* Fermi energy, which decreases as  $r_s$  increases.

### 3.6 GS projections onto site orbitals

We study now the GS projection over the low energy site orbitals shown in Fig. 2, which become the eigenstates when  $r_s \rightarrow \infty$ . More precisely, we consider the first delocalized site SDs having a delocalized center of mass and the same momentum  $\mathbf{K}$  than the GS: The delocalized square  $|S(\mathbf{K})\rangle$ , the 2 delocalized parallelograms  $|P_1(\mathbf{K}, J)\rangle$ , the 2 delocalized parallelograms  $|P_2(\mathbf{K}, J)\rangle$ , and the 4 delocalized deformed squares  $|DS(\mathbf{K}, J)\rangle$ . Fig. 6 shows the behaviors of the GS projections

$$P_\infty^0(r_s) = |\langle \Psi_0(r_s) | S(\mathbf{K}) \rangle|^2 \quad (14)$$

$$P_\infty^1(r_s) = \sum_{J=1}^2 |\langle \Psi_0(r_s) | P_1(\mathbf{K}, J) \rangle|^2 \quad (15)$$

$$P_\infty^2(r_s) = \sum_{J=1}^2 |\langle \Psi_0(r_s) | P_2(\mathbf{K}, J) \rangle|^2 \quad (16)$$

$$P_\infty^3(r_s) = |\langle \Psi_0(r_s) | DS(\mathbf{K}, J) \rangle|^2, \quad (17)$$

where  $\mathbf{K}$  is the GS momentum ( $\mathbf{K} \neq 0$  below  $r_s^F$  and  $\mathbf{K} = 0$  above  $r_s^F$ ).

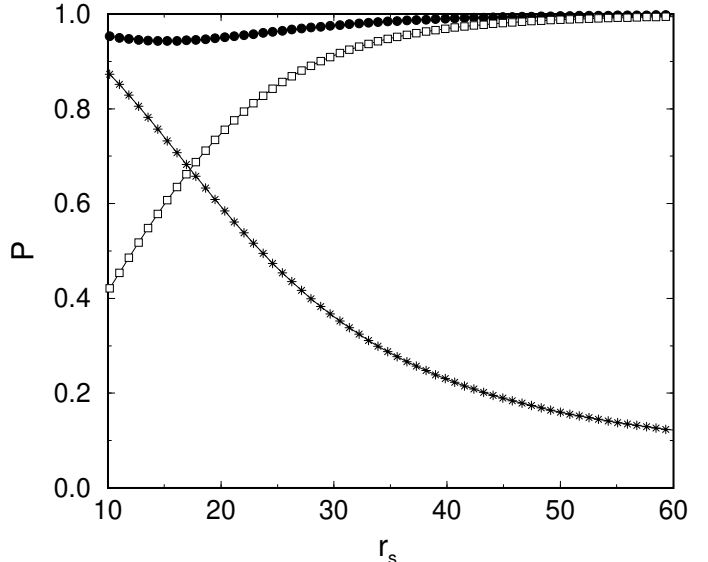


**Fig. 7.** GS projection  $P_0(r_s)$  (\*) over the 20  $\mathbf{K} = 0$  plane wave SDs of low energy,  $P_\infty(r_s)$  (□) over the 9  $\mathbf{K} = 0$  delocalized site SDs and  $P_t(r_s)$  (●) over combined plane wave and site SD re-orthonormalized basis.

While a  $\mathbf{K} \neq 0$  GS has negligible projections over the low energy site SDs of same  $\mathbf{K}$  below  $r_s^F$ , there is an important contribution above  $r_s^F$  of the deformed squares, of the square and of the parallelograms 1 of  $\mathbf{K} = 0$ . As  $r_s$  increases, the GS projection  $P_\infty^0(r_s)$  over the square molecule of  $\mathbf{K} = 0$  goes to 1. The GS projection  $P_\infty^3(r_s)$  over the 4 deformed squares of  $\mathbf{K} = 0$  is the main projection below  $r_s \approx r_s^W$ , a threshold value where the GS projection  $P_\infty^1(r_s)$  over the parallelograms 1 is maximum. One concludes that above  $r_s^F$ , the missing part of the system, which is not described by the low energy unpaired fermions of the previous section, is a floppy Wigner molecule, mainly made of deformed squares below  $r_s^W$  and of squares above  $r_s^W$ .

### 3.7 GS projections onto a combined basis of plane waves and site orbitals

The site SDs and plane wave SDs are not orthonormal. After re-orthonormalization, the total GS projection  $P_t(r_s)$  over the subspace spanned by the 20 plane wave SDs and the 9 delocalized site SDs of low energy and of momentum  $\mathbf{K} = 0$  is given in Fig. 7, together with the GS projection  $P_0(r_s) = P_0^1(r_s) + P_0^4(r_s)$  over the 20 plane wave SDs and  $P_\infty(r_s) = \sum_{I=0}^3 P_\infty^I(r_s)$  over the 9 delocalized site SDs of momentum  $\mathbf{K} = 0$ . One can see that more than 95/100 of the intermediate GS is located inside this combined subspace, suitable to describe a floppy solid co-existing with low energy unpaired fermions. This demonstrates the Andreev-Lifshitz conjecture for the considered mesoscopic lattice model.

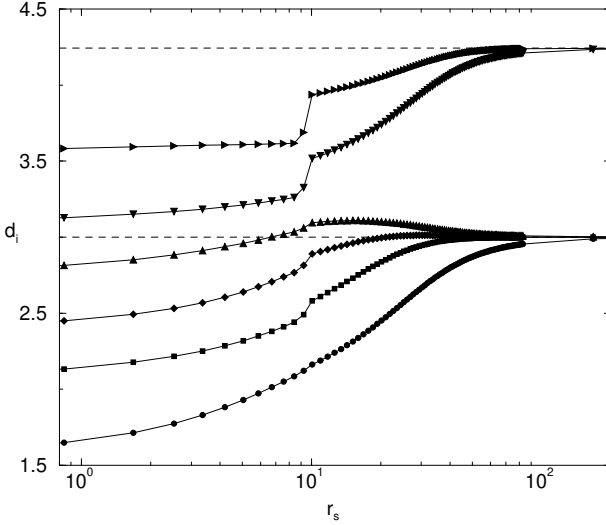


**Fig. 8.** Disorder average of the 6 mean inter-particle spacings  $\langle d(p) \rangle$  as a function of  $r_s$ .

### 3.8 Inter-particle spacings

To understand the nature of the intermediate GS, we study the distribution of the different inter-particle spacings. For the site SDs  $c_i^\dagger c_j^\dagger c_k^\dagger c_l^\dagger |0\rangle$ , one defines the 6 spacings  $d_{ijkl}(1) \leq d_{ijkl}(2) \leq \dots \leq d_{ijkl}(6)$  of each configuration  $ijkl$  ordered by increasing values. The  $n^{th}$  moment  $d^n(p)$  of the  $p^{th}$  GS inter-particle spacing at  $r_s$  is given by:

$$\langle d^n(p) \rangle = \sum_{ijkl=1}^{N_H} d_{ijkl}^n(p) |\langle \Psi_0(r_s) | c_i^\dagger c_j^\dagger c_k^\dagger c_l^\dagger |0\rangle|^2. \quad (18)$$

Weak random potentials are included to get rid of the symmetries of the  $6 \times 6$  lattice. After average over an ensemble of random configurations, we show in Fig. 8 how the 6 mean GS inter-particle spacings  $\langle d_p \rangle$  vary as a function of  $r_s$  for a very weak value  $W = 0.1$  of the disorder strength. When  $r_s \rightarrow \infty$ , the  $3 \times 3$  Wigner molecule gives  $d_1 = d_2 = d_3 = d_4 = 3$  and  $d_5 = d_6 = 3\sqrt{2}$ . As  $r_s$  decays, one can see that one of the largest spacing out of two and two of the smallest spacing out of four remain close their asymptotic values, in contrast to the others. This shows us that one has for intermediate  $r_s$  a floppy solid made of three particles, while the fourth particle remains delocalized. A similar conclusion was drawn from a study of the case  $N = 3$  and  $L = 6$  in Ref. [20], where the intermediate GS was shown to be a floppy two particle molecule co-existing with a third delocalized particle.

The behaviors of the relative fluctuations

$$u_d(p) = \sqrt{\frac{\langle d^2(p) \rangle}{\langle d(p) \rangle^2} - 1} \quad (19)$$

of the 6 inter-particle spacing  $d(p)$  are given in Fig. 9. When  $r_s \rightarrow \infty$ , the fluctuations of the square molecule can be calculated using the  $t/U$  lattice expansion. At first

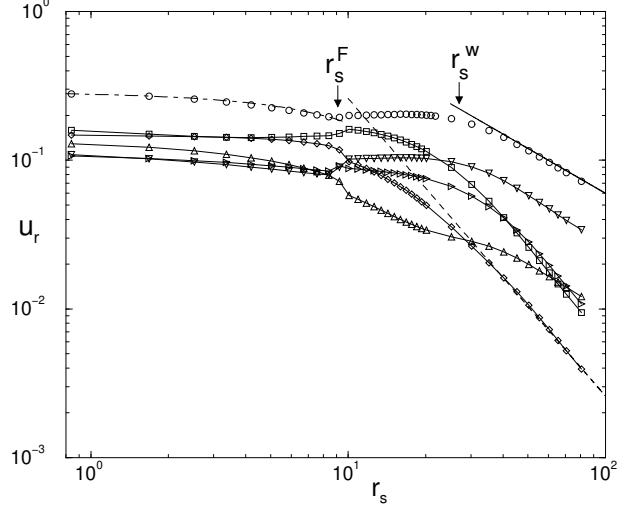


**Fig. 9.** Disorder average of the relative fluctuations  $\langle u_d(i) \rangle$  of the 6 inter-particle spacings as a function of  $r_s$ , using the same symbols as in Fig. 8. Characteristic behaviors  $u_r = 0.28 - 0.01r_s$  (dotted-dashed),  $u_r \propto 6/r_s$  (solid) and  $u_r \propto 26/r_s^2$  (dashed). Note the three spacings having an almost  $r_s$  independent fluctuations for  $r_s^F < r_s < r_s^W$ .

order, one can move only a single particle, which modifies three inter-particle spacings out of six. The fluctuations of the three remaining spacings is obtained by moving two particles, which requires to go to the second order. This explains the three  $r_s^{-1}$  decays and the three  $r_s^{-2}$  decays characterizing the correlated lattice regime. The behaviors in the intermediate regime are remarkable:

- The relative fluctuations of three spacings out of six decay as  $r_s$  increases, as one can expect if a floppy 3 particle molecule becomes more rigid as  $r_s$  increases.
- The three others spacings have relative fluctuations which are nearly independent of  $r_s$  between  $r_s^F$  and  $r_s^W$ , as one can expect if the 4<sup>th</sup> particle remains delocalized.
- Notably, the smallest spacing have a relative fluctuation which varies as  $0.28 - 0.01r_s$  for  $r_s < r_s^F$  (weak coupling regime), which is almost independent of  $r_s$  for  $r_s^F < r_s < r_s^W$  (intermediate regime) before decreasing as  $6/r_s$  above  $r_s^W$  (correlated lattice regime).

The behaviors of the different inter-particle spacings are consistent with the Andreev-Lifshitz conjecture for the considered mesoscopic lattice model. Notably, the number of crystal lattice sites is indeed smaller than the total number of particles.

### 3.9 GS response to small perturbations

We study now the GS response to small perturbations, when the site potentials are non random ( $W = 0$ ), which gives us other signatures of the intermediate regime.

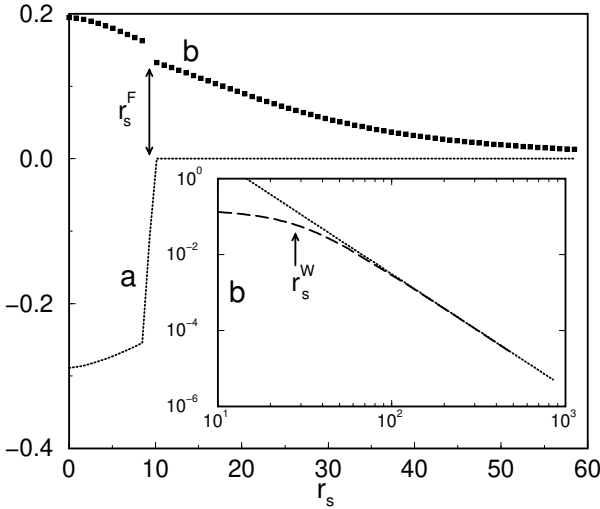


**Fig. 10.** Functions  $a(r_s)/t$  (dotted) and  $b(r_s)/t$  (filled squares) characterizing the GS response to an infinitesimal flux; inset :  $b(r_s)/t$  (dashed) and  $8D/9r_s^{-3}$  (dotted).

### 3.9.1 Aharonov-Bohm flux

The first one consists in piercing the 2d torus by an infinitesimal positive flux  $\phi$  (periodic BCs along the  $y$  direction,  $t \rightarrow t \exp(i\phi/L)$  for hopping along the  $x$ -direction only,  $\phi = \pi$  corresponding to anti-periodic BCs). The coefficients  $a(r_s)$  and  $b(r_s)$  (Kohn curvature) of the expansion  $E_0(r_s, \phi) \approx E_0(r_s, 0) + a(r_s)\phi + b(r_s)\phi^2/2$  are given in Fig. 10. When  $r_s = 0$ ,  $\phi$  removes the fourfold degeneracy of  $E_0$ ,  $a = -\sqrt{3}t/6$  and  $b = 7t/36$ . When  $r_s$  is large, the substitution  $K_x(I) \rightarrow K_x(I) + 2\phi/3$  in Eq. 11 gives  $a = 0$  and  $b \approx 8Dtr_s^{-3}/9$ . An infinitesimal positive flux  $\phi$  gives rise to a persistent current  $I_x = -\partial E_0/\partial\phi = -a$  when  $r_s < r_s^F$  while the GS curvature  $b$  exhibits a smooth crossover between two regimes around  $r_s^W$  (inset of Fig. 10).

### 3.9.2 Single pinning well

The second perturbation consists in introducing a weak negative potential  $V_p$  at a single lattice site  $p$ . The GS density

$$D_p(r_s) = \langle \Psi_0(r_s) | c_p^\dagger c_p | \Psi_0(r_s) \rangle \quad (20)$$

at the site  $p$  is shown in Fig. 11. If  $V_p = 0$ ,  $D_p(r_s = 0) = 1/9$ . A weak negative value of  $V_p$  yields a larger value for  $D_p(r_s = 0)$ . When one turns on the interaction,  $D_p$  first increases and drops at  $r_s^F$ , where the interacting GS begins to have a weaker response to a weak pinning well than the non interacting GS. When  $r_s$  is large,  $D_p$  increases again and the Wigner molecule is pinned. This surprisingly weak response for intermediate  $r_s$  suggests that the system may very weakly respond to the presence of weak impurities. Let us underline that this is precisely for those values of  $r_s$  that the new 2d metal has been observed in 2d field effect devices [5].

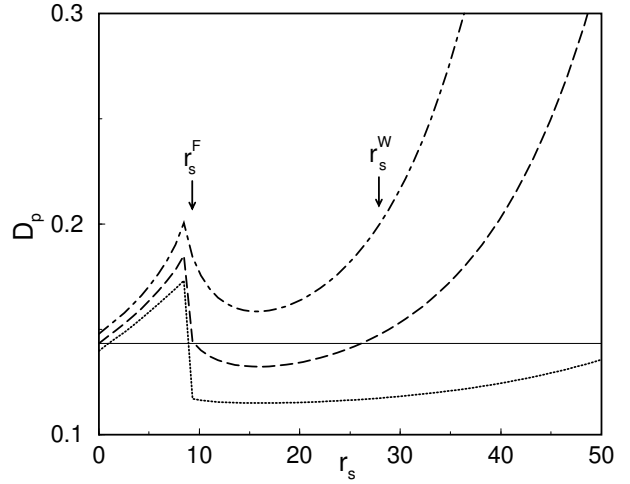


**Fig. 11.** GS density  $D_p(r_s)$  at the pinning site  $p$  with  $V_p/t = -0.01$  (dotted),  $-0.05$  (dashed) and  $-0.1$  (dot-dashed).

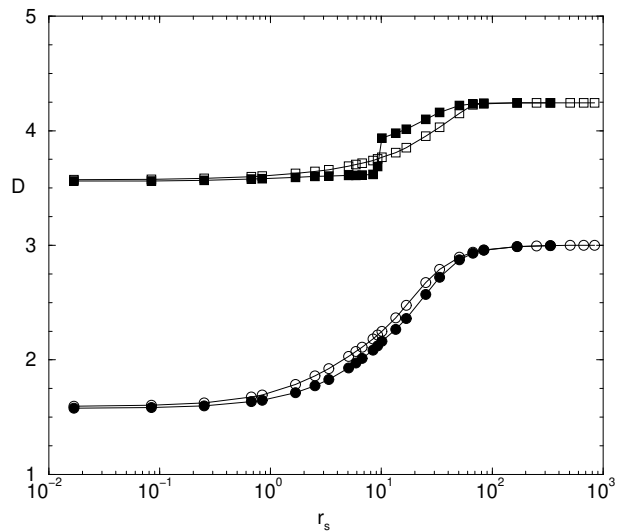


**Fig. 12.** Disorder average of the mean smallest and largest inter-particle spacings for  $W = 0.1$  (filled symbols) and  $5$  (empty symbols) as a function of  $r_s$ .

## 4 Lattice model with random potentials

We extend our study of the disorder by increasing  $W$  from the previously considered weak value ( $W = 0.1$ ) up to larger values ( $W \rightarrow 5$ ) which are too small for having exponential localization of the one particle states on a scale  $L = 6$ , but sufficient for having one particle diffusion.

### 4.1 Inter-particle spacings

In Fig. 12, one can compare the mean smallest and largest inter-particle spacings. For  $W = 0.1$ , the effect of the level crossing at  $r_s^F$  is still visible when one follows the largest spacing, but becomes very smooth for the smallest spacing. The jump associated to  $r_s^F$  is totally smeared for  $W = 5$ . One can also see that the smallest spacing is

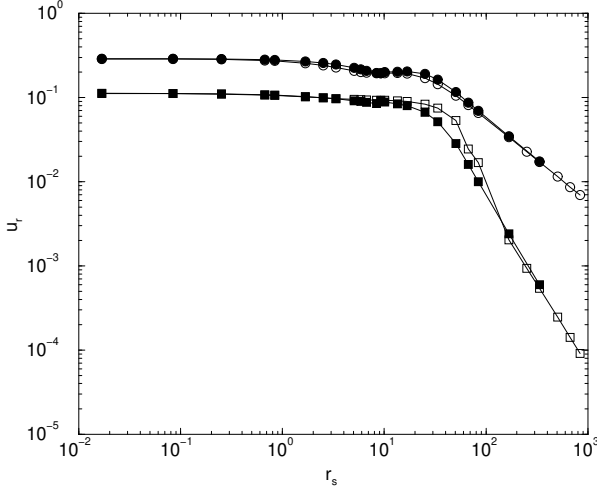


**Fig. 13.** Disorder average of the relative fluctuations of the smallest and largest inter-particle spacings as a function of  $r_s$  for  $W = 0.1$  and  $5$  (same symbols as in Fig. 12).

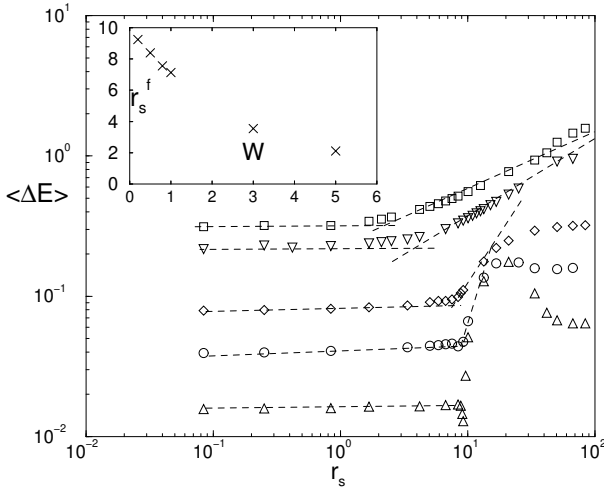


**Fig. 14.** Ensemble average of the first energy spacing  $\langle \Delta E \rangle = \langle E_1 - E_0 \rangle$  as a function of  $r_s$  for  $W = 0.2$  ( $\triangle$ ),  $0.5$  ( $\circ$ ),  $1$  ( $\diamond$ ),  $3$  ( $\nabla$ ) and  $5$  ( $\square$ ). Inset: crossover values  $r_s^F(W)$  as a function of  $W$ .

closer to its asymptotic value  $3$  as one increases  $W$ , showing that disorder favors the formation of a correlated glass. In contrast, the disorder defavors the formation of a perfect crystalline array, the largest spacing requiring a larger  $U$  to reach its asymptotic value  $3\sqrt{2}$ . Similar conclusion can be drawn from Fig. 13 where the corresponding relative fluctuations of the smallest and largest spacings are given.

## 4.2 First energy excitation

Fig. 14 gives the average over the disorder of the first energy spacing  $\langle \Delta E \rangle = \langle E_1 - E_0 \rangle$  as a function of  $r_s$  for different values of  $W$ . One can see a weak coupling regime where  $\langle \Delta E \rangle$  does not depend on  $r_s$ , followed by an increase

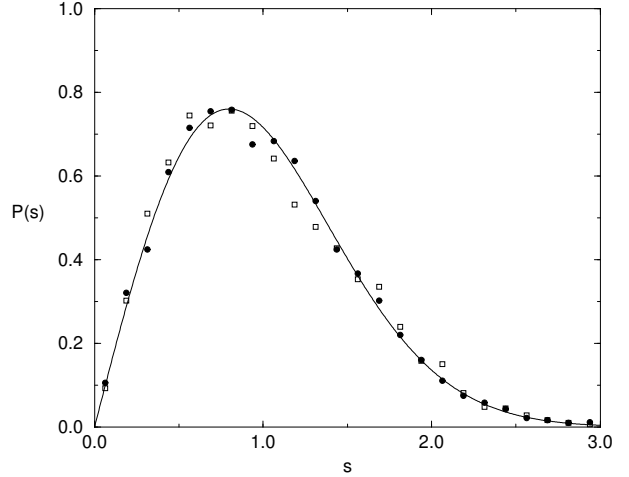


**Fig. 15.** Distribution  $P(s)$  of the first energy excitation  $s = E_1 - E_0 / \langle E_1 - E_0 \rangle$  for  $W = 5$  and  $r_s = 1.7$  ( $\bullet$ ) and  $r_s = 5$  ( $\square$ ). The solid line is the Wigner surmise  $P_W(s)$ .

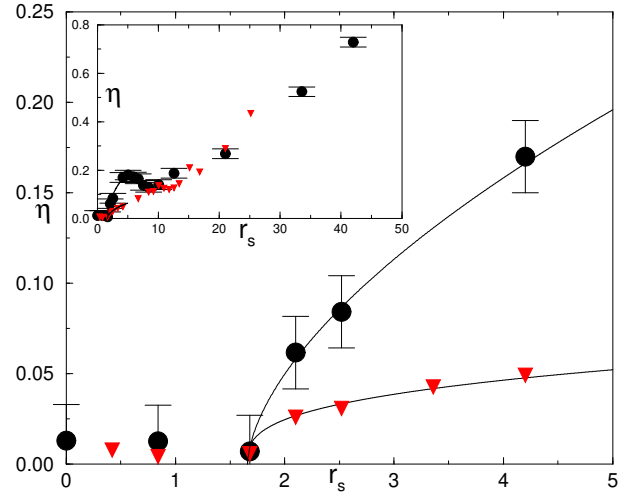


**Fig. 16.** Spectral parameter  $\eta$  for the first energy spacing as a function of  $r_s$  for  $W = 3$  ( $\blacktriangledown$ ) and  $5$  ( $\bullet$ ), showing the sharp breakdown of the Wigner distribution at  $r_s^F \approx 1.7$ . The inset shows that the level repulsion is totally suppressed when  $r_s \rightarrow \infty$ .

of  $\langle \Delta E \rangle$  as a function of  $r_s$ . The threshold coupling between those two regimes is naturally of the order of  $r_s \approx 10$  when  $W$  is small. When  $W$  is larger,  $\langle \Delta E \rangle \propto r_s^\alpha$  as indicated by the dashed lines of Fig. 14. Assuming that the correlated regime occurs at the ratios  $r_s^F(W)$  below which  $\langle \Delta E \rangle$  does not depend on  $r_s$ , and above which  $\langle \Delta E \rangle$  increases as  $r_s^\alpha$ , we have plotted in the inset of Fig. 14 how  $r_s^F(W)$  depends on  $W$ . The onset  $r_s^F(W)$  of the correlation effects decays from the value  $\approx 10$  where there is a level crossing without disorder towards a much smaller value when  $W \rightarrow 5$ .

This onset  $r_s^F(W)$  for  $W = 3 \dots 5$  can also be seen in the sample-to-sample distribution of the first energy excitation. When  $r_s$  is weak, the first many body excitation corresponds to a single one body excitation above the

Fermi energy. If the one body motion is diffusive, the one body spectrum is correlated, and the distribution  $P(s)$  of the energy spacing between consecutive levels is given by the Wigner surmise  $P_W(s)$ . Therefore, the first many body spacing  $s = E_1 - E_0 / \langle E_1 - E_0 \rangle$  measured in units of its ensemble averaged value is given by the Wigner surmise:

$$P_W(s) = \frac{\pi s}{2} \exp\left(-\frac{\pi s^2}{4}\right) \quad (21)$$

as one can see in Fig. 15 for  $r_s < r_s^F(W)$ . When  $r_s$  exceeds  $r_s^F(W)$ , the level repulsion becomes weaker. As shown in Fig. 15,  $P(s)$  for low  $s$  is systematically larger than  $P_W(s)$  when  $r_s = 5$ . To study this weakening of the spectral rigidity, we define a spectral parameter

$$\eta(r_s) = \frac{\int_0^a (P(s) - P_W(s)) ds}{\int_0^a (P_P(s) - P_W(s)) ds}, \quad (22)$$

where  $P_P(s) = \exp -s$  is the Poisson distribution characterizing uncorrelated levels and  $a = 0.4729$  is the value where  $P_W(a) = P_P(a)$ .  $\eta = 1$  when  $P(s) = P_P(s)$  and  $\eta = 0$  when  $P(s) = P_W(s)$ . Very remarkably, one can see in Fig. 16 that the first energy excitation is well described by the Wigner surmise up to a threshold consistent with  $r_s^F(W)$  where the spectral rigidity suddenly becomes weaker. The curves  $\eta(r_s)$  are given on a larger interval of values of  $r_s$  in the inset of Fig. 16, and one can see the two characteristic thresholds detected in earlier studies [10,11] for  $W = 5$ :  $r_s^F(W = 5) \approx 2$  where one has the breakdown of Wigner-Dyson rigidity and  $r_s^W(W = 5) \approx 10$  where was located the onset of charge crystallization.

In summary, when disorder yields one particle diffusion, the onset of correlation effects occurs at a weaker value  $r_s^F(W)$  than in the clean limit, yielding for the excitation energy  $\Delta E$  an increase of its average value when  $r_s$  increases and a change of its distribution.

### 4.3 Breakdown of the Hartree-Fock approximation

A last evidence proving that  $r_s^F(W)$  is indeed the onset of the correlation effects is shown by Fig. 17 where the disorder average total GS persistent current  $\langle I_x \rangle$  enclosing a flux  $\phi = \pi/2$  is shown as a function of  $r_s$ . Both the exact numerical value and the mean field value given by the Hartree-Fock approximation are given. As one can see, the change seen in the mean and in the distribution of the first energy excitation at  $r_s^F(W)$  is correlated with the fact that the ground state cannot be described by the best possible Slater determinant (HF-approximation), due to correlation effects which are beyond a simple mean field approach.

## 5 Conclusion

It is interesting to compare our results obtained in a 2d torus without edge to those obtained using an harmonic confinement. For instance, a Monte Carlo study [22] of a

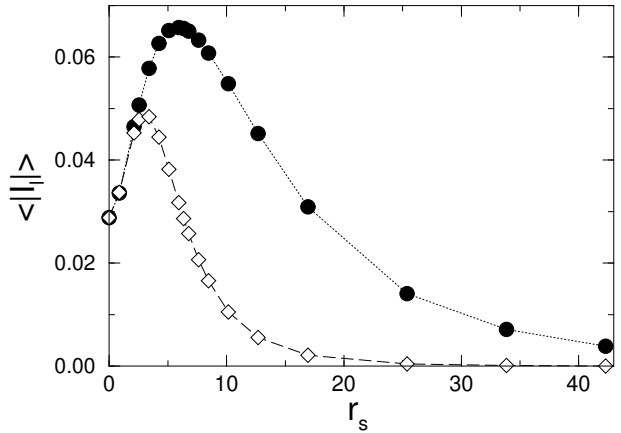


**Fig. 17.** Ensemble average GS current  $\langle I_x \rangle$  as a function of  $r_s$  for  $W = 5$ . Exact values (filled symbols) and HF values (empty symbols).

few electrons in an harmonic trap concludes that mesoscopic Wigner crystallization proceeds in two stages: (i) via radial ordering of electrons on shells and (ii) freezing of the intershell rotation. This crystallization in two steps, with a particular intermediate behavior, could be attributed to the non uniform density characterizing the harmonic trap. One may argue that crystallization takes place in the low density edges before the large density bulk, such that this intermediate regime might be related to some interplay between edge and bulk effects. We find that mesoscopic Wigner crystallization takes also place in two stages when the particles are confined on a 2d torus with a uniform density. This raises the question to know if this intermediate regime is a pure mesoscopic effect valid only in small systems, or the mesoscopic trace on the vacancy-solid phase proposed by Andreev and Lifshitz, where unpaired fermions with reduced Fermi energy co-exist with a floppy solid. We believe that the results given by this study favors the second possibility, and we suggest that the understanding of its associated transport properties may be useful for explaining the 2d metal observed in various 2d field effect devices for similar ratios  $r_s$ . Upon completion of this manuscript, we received from Boris Spivak [23] a preprint where the existence of an intermediate phase between the Fermi liquid and the Wigner crystal is claimed to be a generic property of the 2d pure electron liquid in MOSFETs at zero temperature, and where the consequences for the experimental results obtained in 2d MOSFETs are discussed.

We thank G. Benenti for the calculation of the H-F persistent currents in subsection 4.3, B. Spivak and J.-P. Bouchaud for drawing our attention onto Refs. [14] and [19] respectively and Z. Á. Németh for stimulating discussions. G. Katomeris acknowledges the financial support provided through the European Community's Human Potential Programme under contract HPRN-CT-2000-00144.

## References

1. B. Tanatar and D.M. Ceperley, Phys. Rev. B **39**, 5005 (1989).
2. M. Imada and M. Takahashi, J. Phys. Soc. Jpn. **53**, 3770 (1984).
3. Ladir Cândido, Philip Philipps and D. M. Ceperley, Phys. Rev. Lett. **86**, 492 (2001).
4. D. Varsano, S. Moroni and G. Senatore, Europhys. Lett. **53**, 348 (2001).
5. E. Abrahams, S. V. Kravchenko and M. P. Sarachik, Rev. Mod. Phys. **73**, 251 (2001) and refs therein.
6. J. H. Schön, S. Berg, Ch. Kloc and B. Batlogg, Science **287**, 1022 (2000).
7. R. C. Ashoori, Nature **379**, 413 (1996); Tarucha S et al., Phys. Rev. Lett. **77**, 3613 (1996); J. Kyriadidis et al., cond-mat/0111543.
8. D. H. Dubin and T. M. O'Neil, Rev. Mod. Phys. **71**, 87 (1999).
9. C. Yannouleas and U. Landman, Phys. Rev. Lett. **85**, 1726 (2000).
10. G. Benenti, X. Waintal and J.-L. Pichard, Phys. Rev. Lett. **83**, 1826 (1999).
11. G. Benenti, X. Waintal and J.-L. Pichard, Europhys. lett. **51**, 89 (2000).
12. F. Selva and J.-L. Pichard, Europhys. Lett. **55**, 518 (2001).
13. M. Martinez and J.-L. Pichard, cond-mat/0203579.
14. A. F. Andreev and I. M. Lifshitz, Sov. Phys. JETP **29**, 1107 (1969).
15. B. Castaing and P. Nozieres, J. Phys. France **40**, 257 (1979).
16. G. G. Batrouni and R. T. Scalettar, Phys. Rev. Lett. **84**, 1599 (2000).
17. I. E. Dzyaloshinskii, P. S. Kondratenko and V. S. Levchenkov, Sov. Phys. JETP **35**, 823 (1972); ibid **35**, 1213 (1972).
18. B. Shapiro, Phil. Mag. **B**, 1303 (2001).
19. J. P. Bouchaud and C. Lhuillier, Europhys. Lett. **3** 481 (1987) and Europhys. Lett. **3** 1273 (1987); J. P. Bouchaud, A. Georges and C. Lhuillier, J. Phys. France **49** 553 (1988).
20. Z. Á. Németh and J.-L. Pichard, Europhys. Lett. **58**, 744 (2002).
21. E. Wigner, Trans. Faraday Soc. **34**, 678 (1938).
22. A. V. Filinov, M. Bonitz and Yu. E. Lozovik, Phys. Rev. Lett. **86**, 3851 (2001).
23. B. Spivak, unpublished. See however B. Spivak, Phys. Rev. B **64** 85317 (2001).